Attenuating ABHD17 isoforms augments the *S*-acylation and function of NOD2 and a subset of Crohn's disease-associated NOD2 variants.

Short title: Inhibiting ABHD17 promotes NOD2 activity.

Charneal L. Dixon[1,2], Noah R. Martin[1], Micah J. Niphakis[3], Benjamin F. Cravatt[4], Gregory D. Fairn[1,2,5]**

[1]Department of Pathology, Dalhousie University, Halifax, NS, Canada
[2]Keenan Research Centre for Biomedical Science, St. Michael's Hospital, Unity Health Toronto, Toronto, ON, Canada
[3]Lundbeck La Jolla Research Center, Inc., San Diego, CA, USA
[4]Department of Chemistry, The Scripps Research Institute, La Jolla, CA, USA
[5]Department of Biochemistry and Molecular Biology, Dalhousie University, Halifax, NS, Canada

Grant Support: This work was supported by a Project Grant from the Canadian Institutes of Health Research (grant no.: PJT166010; to G.D.F.), an Innovator Award from the Kenneth Rainin Foundation, and a grant from the National Institutes of Health, (R01CA193994 to B.F.C). A Tier 1 Canada Research Chair supports G.D.F. in Multiomics of Lipids and Innate Immunity. C.L.D. was supported by a Breakthrough Accelerator Fellowship from the Dalhousie Medical Research Foundation/Medical Research Development Office. N.M is a recipient of a graduate scholarship from the I3V Wave and the Dalhousie Medical Research Development Office.

**To whom correspondence should be addressed: Gregory D. Fairn, Department of Pathology, Dalhousie University, Sir Charles Tupper Medical Building, Room 11B, 5850 College Street, PO Box 15000, Halifax, Nova Scotia, Canada B3H 4R2.
Telephone: 902-221-3719. Email: gfairn@dal.ca

Disclosures:
The authors declare that the research was conducted in the absence of any commercial or financial relationships that could be construed as a potential conflict of interest.

SYNOPSIS

The peptidoglycan sensor NOD2 requires post-translational *S*-acylation to associate with cellular membranes and transduce signals. This study identified the ABHD17 family of thioesterases as responsible for NOD2 deacylation and inactivation. Inhibiting or

silencing ABHD17 isoforms increases *S*-acylation and functionality of NOD2 and a subset of Crohn's disease-associated variants.

ABSTRACT

BACKGROUND AND AIMS: NOD2 is an intracellular innate immune receptor that detects bacterial peptidoglycan fragments. Although nominally soluble, some NOD2 is associated with the plasma membrane and endosomal compartments for microbial surveillance. This membrane targeting is achieved through post-translational *S*-acylation of NOD2 by the protein acyltransferase ZDHHC5. Membrane attachment is necessary to initiate a signaling cascade in response to cytosolic peptidoglycan fragments. Ultimately, this signaling results in the production of antimicrobial peptides and proinflammatory cytokines. In most cases, *S*-acylation is a reversible post-translational modification with removal of the fatty acyl chain catalyzed by one of several acyl protein thioesterases. Deacylation of NOD2 by such an enzyme will displace it from the plasma membrane and endosomes, thus preventing signaling.

METHODS: To identify the enzymes responsible for NOD2 deacylation, we used engineered cell lines with RNA interference and small-molecule inhibitors. These approaches were combined with confocal microscopy, acyl-resin-assisted capture, immunoblotting, and cytokine multiplex assays.

RESULTS: We identified α/β-hydrolase domain-containing protein 17 isoforms (ABHD17A, ABHD17B, and ABHD17C) as the acyl protein thioesterases responsible for NOD2 deacylation. Inhibiting ABHD17 increased the plasma membrane localization of wild-type NOD2 and a subset of poorly acylated Crohn's disease-associated variants.

This enhanced NOD2 activity, increasing NF-κB activation and pro-inflammatory cytokine production in epithelial cells.

CONCLUSIONS: These findings demonstrate that ABHD17 isoforms are negative regulators of NOD2. The results also suggest that targeting ABHD17 isoforms could restore functionality to specific Crohn's disease-associated NOD2 variants, offering a potential therapeutic strategy.

KEYWORDS: Crohn's disease, NOD2, *S*-acylation, Acyl Protein Thioesterase, ABHD17, Inflammation, IL-8

INTRODUCTION

Crohn's disease (CD) is a prominent form of inflammatory bowel disease that can affect any segment of the gastrointestinal tract, extending from the mouth to the anus, that most commonly manifests in the lower portion of the small intestine and the upper colon. CD is characterized by a range of symptoms, including weight loss, fatigue, diarrhea, and abdominal pain, which can be debilitating and, in some instances, life-threatening. Current treatments, including the use of steroids and tailored dietary approaches, have proven effective in alleviating these symptoms and forestalling disease exacerbations. Despite these advances, CD remains an intricately multifactorial condition influenced by genetic predisposition, environmental factors, dietary habits, and an individual's unique microbiome.

The nucleotide-binding oligomerization domain-containing protein 2 (NOD2) gene has been consistently implicated in the pathogenesis of CD since it was first identified in 2001 [1-3]. NOD2 is a member of the evolutionarily conserved family of NOD-like receptors (NLR) that provide intracellular surveillance through detecting cytoplasmic

pathogen-associated molecular patterns [4-6]. NOD2 belongs to the NLRC subfamily, containing two amino-terminal caspase activation and recruitment domains (CARD) [7]. NOD2, and the closely related NOD1, bind small peptides originating from bacterial peptidoglycan. The binding of ATP and peptidoglycan fragments to NOD2 induces conformational changes and oligomerization, engaging receptor-interacting protein kinase 2 (RIPK2) and triggering a cascade of ubiquitination and phosphorylation events. This process activates the nuclear factor kappa B (NF-κB) and mitogen-activated protein kinases (MAPK) pathways, ultimately inducing the transcription of pro-inflammatory cytokines, chemokines, and other inflammatory mediators [8, 9].

The complex pathophysiology of CD has led to the emergence of multiple functional roles for NOD2. In the presence of a diverse and healthy microbiome, NOD2 is thought to provide signals that facilitate the expression and secretion of small anti-microbial peptides (AMPs) such as α- and β-defensins by Paneth cells and other epithelial cells of the small and large intestine [10, 11]. Thus, loss of NOD2 function and a reduction in AMPs can lead to changes in the microbiome and dysbiosis. This shift in the bacterial population and activity can result in an increase in bacteria capable of damaging or invading the epithelial lining. In this instance, NOD2, in combination with ATG16L1, another CD risk factor, is critical in initiating an anti-bacterial autophagic pathway in response to invasion [12-14]. Finally, NOD2 can be exposed to peptidoglycan in resident macrophage and epithelial cells through its uptake via the SLC15A family of transporters in the plasma membrane (PM) and endosomes to initiate inflammatory cytokine production [15-17]. However, precisely how loss of NOD2

contributes to the development of CD remains unclear, although it may impair the ability to recover from acute infections, as observed in murine models [18].

In contrast to toll-like receptors that recognize extracellular or luminal bacterial components, NOD2 is an intracellular receptor that attaches to the surface of the PM and endomembranes to transduce signals following binding to phosphorylated muramyl dipeptide (MDP) in the cytosol [17, 19]. Previously it was demonstrated that *S*-acylation (often called *S*-palmitoylation or palmitoylation), was required to target NOD2 and NOD1 to membranes [20, 21]. It was further revealed that the protein acyltransferase ZDHHC5 mediates the attachment of the fatty acyl group to NOD2 (Cys395 and 1033) and NOD1 (Cys558, 567, 952); this modification is critical for the ability of NOD proteins to respond to peptidoglycan components and mount an effective inflammatory response [21]. Additionally, several CD-associated loss-of-function variants of NOD2 exhibit reduced levels of *S*-acylation, referred to as hypo-acylation. The *S*-acylation deficiency correlates with decreased signaling in response to peptidoglycan for these hypo-acylated variants. As *S*-acylation is a reversible post-translational modification, we theorized that identifying and inhibiting the responsible acyl protein thioesterase(s) could potentially enhance the *S*-acylation of not only wild-type NOD2 but also hypo-acylated mutants. Indeed, such an intervention could improve the functionality of some of the CD-associated NOD2 variants.

In this study, we identify the family of □/□-hydrolase domain-containing protein 17 (ABHD17A, 17B, 17C) as the enzymes responsible for the deacylation of NOD2. Furthermore, we find that inhibiting ABHD17 enzymes partly restores the localization, *S*-

acylation, and ligand-induced signaling of a subset of CD-associated loss-of-function NOD2 variants.

RESULTS

Deacylation of NOD2 is Enzymatically Mediated

Unlike other types of protein lipidation, the covalent attachment of palmitate and other fatty acids to cysteine residues via a thioester bond is reversible [22]. Dynamic changes in *S*-acylation status play a role in the regulation and function of proteins [23-25]. Indeed, the proportion of NOD2 that are *S*-acylated is increased in response to stimuli [21]. Yet, to date, nothing is known about the reversibility of this modification on NOD2 or the identity of an acyl protein thioesterase (deacylating) enzyme.

To determine if colorectal epithelial cells express a thioesterase capable of deacylating NOD2, we first developed a cell model with controllable low-level expression of GFP-NOD2. To do this, we used the Sleeping Beauty transposon system to engineer HCT116 and HT29 epithelial cell lines with a doxycycline-inducible GFP-tagged NOD2 (GFP- NOD2) as described in the Methods. Following the generation and selection of the polyclonal cell line, doxycycline-inducible expression of GFP-NOD2 was confirmed by immunoblotting and microscopy (Figure 1*A*, *B*). In these cells, there was a sizeable cytosolic pool of GFP-NOD2 and a smaller fraction associated with the PM, consistent with previous results [21, 26, 27]. Palmostatin B is a cell-permeable, broad-spectrum inhibitor of acyl protein thioesterases, including acyl protein thioesterase (APT) 1 and 2 [28, 29], palmitoyl-protein thioesterase 1 [29], α/β-hydrolase domain (ABHD) 6 [30], ABHD10 [31] ABHD12 [32], ABHD16A [30, 33] and ABHD17(A/B/C) [30]. Thus, we next treated cells expressing GFP-NOD2 with either solvent control (DMSO)

or Palmostatin B for 4 h. Following the 4 h incubation with Palmostatin B, confocal microscopy revealed a significant enrichment of the GFP-NOD2 on the PM ($p<0.0001$) (Figure 1*C-E)*.

Since it was previously demonstrated that the NOD2^{C395,1033S} S-acylation deficient mutant is completely cytosolic [20, 21], we reasoned that the observed plasmalemmal enrichment was due to a more substantial fraction of GFP-NOD2 being *S*-acylated. To confirm that Palmostatin B increases S-acylation of NOD2 experimentally, we used an acyl resin-assisted capture (acyl-RAC) technique (Figure 1*F*, G) that uses a series of steps, including the blockage of free-thiols, cleavage of acyl-thioester bonds, and the use of an affinity matrix to bind the newly liberated and previously *S*-acylated cysteine residues from cell lysates. Immunoblotting GFP-NOD2 following acyl-RAC demonstrated a 3.2-fold increase ($p=0.0192$) in *S*-acylated GFP-NOD2 in HCT116 cells treated with Palmostatin B compared to control (Figure 1*H*). The presence of a signal with hydroxylamine (+HA) treatment indicates that fatty acids are attached to the protein via a thioester bond. These results suggest that *S*-acylation of NOD2 is reversible and that a Palmostatin B-sensitive protein mediates the enzymatic removal of acyl chains from NOD2.

Inhibiting ABHD17 Enzymes Increases NOD2 S-acylation

Motivated by the impact of Palmostatin B on NOD2 localization and *S*-acylation, we used selective small-molecule inhibitors to target known deacylation enzymes to identify the relevant NOD2 thioesterases. HCT116 cells stably expressing GFP-NOD2 were treated with DMSO or inhibitor for a total of 4 h. Treatment with ML348 [34] and

ML349 [34], which target APT1 and APT2, respectively, had no discernable effect on the localization of GFP-NOD2 (Figure 2*A*). A similar lack of response was observed with the selective ABHD6 inhibitor, WWL70 [35, 36]. Conversely, THL [36, 37] and ABD957 [38] treated HCT116 cells have significant enrichment of GFP-NOD2 at the PM, 2.2-fold ($p=0.0175$) and 4.9-fold ($p<0.0001$) increase, respectively (Figure 2*B*). A similar enrichment was observed in HT29 cells ($p<0.0001$) (Figure 2*C*, *D*). For ABD957-treated HCT116 cells, this corresponded to a mean fold increase of 4.4 ($p=0.0061$) in the fraction of *S*-acylated NOD2 compared to DMSO, as determined by the acyl-RAC assay. In contrast, the THL treatment did not significantly impact the amount of *S*-acylated NOD2 protein captured during the assay ($p=0.3455$) (Figure 2*E, F*).

These data suggest that at least one of the ABHD17 isoforms may be the primary enzyme responsible for deacylating NOD2. We further hypothesized that given the homology between NOD1 and NOD2 and that ZDHHC5 is required for the *S*-acylation of both NOD1 and NOD2, the same deacylating enzyme may regulate NOD1. To test this, we treated HCT116 cells stably transfected with doxycycline-inducible GFP-NOD1 with the various thioesterase inhibitors but observed no significant increase ($p>0.05$) in plasma membrane enrichment (Figure 2*G*, *H*). However, given the limited cytoplasmic pool of GFP-NOD1, any observed change in plasma membrane enrichment could be negligible due to the minimal amount of soluble NOD1 available for *S*-acylation.

Overexpression of ABHD17 Enzymes Depletes the Plasmalemmal Pool of NOD1 and NOD2

Having narrowed the list of candidate enzymes using inhibitors, we next examined the cellular consequences of expressing the individual α/β-hydrolases targeted by THL and ABD957. Preventing NOD2 *S*-acylation prevents NOD2 and NOD1 from localizing to the PM [20, 21]. Accordingly, we anticipated that overexpressing an α/β-hydrolase domain enzyme capable of deacylating NOD2 would similarly reduce the fraction of GFP-NOD2 associated with the PM. HCT116 cells stably expressing GFP-NOD2 were transiently transfected with individual ABHD enzymes (6, 12, 16A,17A, 17B and 17C) (Figure 3*A*). The three ABHD17 isoforms significantly redistributed GFP-NOD2 from PM to cytosol, with ABHD17B and 17C being the most effective in this assay (Figure 3*B*). In contrast, overexpression of the THL-sensitive ABHD6, ABHD12, and ABHD16A did not significantly deplete the plasmalemmal GFP-NOD2 signal ($p>0.05$). These data further support ABHD17 isoforms as the primary NOD2 deacylation enzymes. When we applied this strategy to HCT116 cells stably expressing GFP-NOD1 (Figure 3*C*, *D*), we observed a modest ≈ 40%reduction ($p=0.009$) in GFP-NOD1 signal at the PM when ABHD17A was overexpressed. ABHD17B and 17C isoforms were more effective ($p<0.0001$) at redistributing GFP-NOD1 from the PM to cytosol, with ≈ 60% and ≈ 78% decrease, respectively. These results support the notion that ABHD17 isoforms are the relevant deacylating enzymes and, thus, negative regulators of NOD1 and NOD2 function.

Attenuating ABHD17 Increases the Plasmalemmal Enrichment of NOD2

ABHD17 enzymes are ubiquitously expressed in most cell types (Figure *S1A, B*), while NOD2 expression is restricted to immune cells and intestinal epithelial and Paneth

cells [39, 40]. Although this suggests a broader regulatory role for these AHBD17 enzymes, the high expression of ABHD17C in gastrointestinal tissues makes it a key candidate for influencing NOD2 function. The ubiquitous expression of ABHD17 isoforms, particularly the elevated levels of ABHD17C in the gastrointestinal tract, supports its relevance to gastrointestinal immunity. Next, we investigated the effects of silencing the individual ABHD17 on NOD2 *S*-acylation in HCT116 cells. The relative expression of ABHD17 isoforms was analyzed using quantitative polymerase chain reaction (qPCR). All three isoforms have similar mRNA levels in HCT116 cells (Figure 4*A*). Thus, we conducted experiments by knocking down individual isoforms and all three simultaneously. Reverse transcription (RT)-qPCR showed efficient silencing of ABHD17A, 17B, and 17C either individually or in combination 48 hours after introduction of siRNA (Figure 4*B*). Silencing of ABHD17A had no significant effect on NOD2 localization ($p= 0.1306$). However, this siRNA only achieved ~75% reduction in the transcript (Figure 4*C*, *D*), raising the possibility that the lack of effect is due to incomplete silencing. Conversely, knockdown of either ABHD17B or ABHD17C moderately affected GFP-NOD2 membrane localization, resulting in a 1.8-fold ($p=0.0007$) and 1.6-fold ($p=0.0203$) increase, respectively. Notably, the simultaneous knockdown of all three ABHD17 isoforms resulted in a 3.9-fold increase ($p<0.0001$) in GFP-NOD2 associated with the plasma membrane. The increase in the triple knockdown cells (Triple KD) was comparable to cells treated with the selective ABHD17 inhibitor (ABD957) (Figure 2B). The results from overexpression and silencing experiments indicate that the ABHD17 isoforms, particularly ABHD17B and ABHD17C, are the main thioesterases responsible for NOD2 deacylation in HCT116 cells. These

findings are consistent with ABHD17 expression data, which show that ABHD17A, ABHD17B, and ABHD17C are expressed at levels higher than NOD2 (Figure S1).

Attenuating ABHD17 Increases NOD2 Signaling

Next, we examined how inhibiting or silencing ABHD17 would affect endogenous NOD2-dependent activation and downstream pathways. To do this, we monitored the phosphorylation status of downstream effector proteins NF-κB (p65), IκBα, and MAPK (p38) in response to NOD2 – RIPK2 activation (Figure 5*A-D*). Previous research has shown that inhibiting *S*-acylation of NOD2 reduces NF-κB and MAPK activity in RAW267.4 and HCT116 cells stimulated with MDP [21]. Next, HCT116 cells were treated with siRNAs or ABD957, as in Figure 4, before stimulation with a synthetic NOD2 agonist, L18-MDP. As predicted, cells with attenuated ABHD17 and elevated NOD2 *S*-acylation displayed an increase in the activation of NF-κB and MAPK responses (Figure 5*B-D*). Ultimately, this signal transduction cascade results in the upregulation of cytokines; therefore, we examined the secretion of cytokines under these conditions. The knockdown of individual isoforms was insufficient to promote increased interleukin 8 (IL-8), but did result in enhanced granulocyte-macrophage colony-stimulating factor (GM-CSF) production and secretion (Figure 5*E, F*). Silencing all three isoforms further enhanced the production and secretion of both IL-8 and GM-CSF. Again, to complement the siRNA-mediated knockdown experiments, we conducted an additional experiment using ABD957. Cells treated with ABD957 before ligand stimulation secreted ≈ 6-fold ($p<0.0001$) more IL-8 than DMSO-treated HCT116 cells (Figure 5*G*) and ≈ 3-fold ($p<0.0001$) more GM-CSF (Figure 5*H*). Together, these

results demonstrate that the loss of ABHD17 function increases NF-κB and MAPK signaling pathways in response to the NOD2 ligand MDP.

Inhibiting ABHD17 Enzymes Restores Localization and S-acylation of select CD-Associated NOD2 Variants.

Mechanistically, mutations in NOD2 could manifest in loss-of-function in numerous ways. For example, mutations could abrogate MDP binding, RIPK2 binding, ATP binding, or *S*-acylation. Indeed, it was previously reported that several CD-associated NOD2 loss-of-function variants have impaired S-acylation and do not localize to the plasma membrane [21]. Targeted inhibition of ABHD17 enzymes could increase the *S*-acylation of hypo-acylated mutants, potentially improving their ability to respond to MDP. To examine this possibility, we again used the Sleeping Beauty transposon system to create a stable transgenic cell line for each mutant using HCT116 and HEK293T cells. We examined several hypo-acylated variants with mutants spread throughout the protein, including the relatively common R702W and two other less common variants L248R, located between the CARD domains and the NACHT domains, and A755V, located between the NACHT and LRRs. We used confocal microscopy to examine the effects of inhibitors (THL, ABD957 and Palmostatin B) and RNA interference on the subcellular localization of each variant (Figure 6*A*). As we observed with wildtype NOD2, inhibiting ABHD17 increased the recruitment of L248R, R702W, and A755V to the plasma membrane (Figure 6*B-D*). Contrary to what we observed with wildtype NOD2, THL had no significant impact on the localization of the NOD2 mutants ($p>0.05$). We also confirmed that increased plasma membrane

localization was associated with enhanced *S*-acylation (Figure 6*E-H*). These results suggest that some hypo-acylated NOD2 mutants are substrates for the acyltransferase ZDHHC5 and the ABHD17 thioesterase enzymes. Notably, inhibiting the deacylation mediated by the thioesterases increased their respective plasmalemmal localization.

Next, we sought to determine if increasing the targeting for these variants to the plasma membrane influences their ability to signal. For this, we used Sleeping Beauty-engineered stable doxycycline-inducible HEK293T cells, chosen for their minimal to non-existent endogenous NOD2 expression [7, 41], as a model for exploring agonist-induced NF-κB activation and cytokine production. Protein expression was induced with 10 ng/mL doxycycline for 18-20h. We titrated doxycycline to the lowest effective concentration to induce expression while preventing spurious activation of NOD2-mediated NF-κB signaling. Cells were stimulated with 100 ng/mL L18-MDP for 1h after RNA interference or a 4h treatment with ABD957. We show NOD2-RIPK2 activation of NF-κB and MAPK pathways, as in the HCT116 cells, using immunoblotting to capture phosphorylation of IκB and p38 (Figure 7*A-C*). Next, we analyzed the culture medium for pro-inflammatory mediators to correlate these acute stimulations with cytokine release from the HEK293T cells. IL-8 and TNFα were elevated compared with DMSO control (Figure 7*D*, *E*). HEK293T cells stably expressing A755V exhibited significant ($p<0.0001$) 4.1 and 3.4-fold increases in IL-8 and TNFα secretions when cells were stimulated with L18-MDP (Figure 6*D*, *E*). Cells expressing R702W displayed a modest increase in TNFα, and in IL-8 secretion. Cells expressing L248R also displayed a modest, albeit not statistically significant, in TNFα and IL-8 secretions when stimulated with L18-MDP. The results show that inhibiting these hypo-acylated NOD2 variants can

partly increase their localization to the plasma membrane. However, the magnitude of signal transduction is variable at least in this engineered model.

S-acylation deficient NOD2^{L1007fs} and NACHT domain mutants are not improved by ABHD17 inhibition

To better understand the acylation–deacylation cycle and how it may be altered in the different mutants, we next examined the CD-associated 3020insC frameshift mutation that encodes a C-terminally truncated NOD2 protein lacking the last 33 amino acids (L1007fs). This C-terminal truncation mutant lacks Cys1033, one of the two S-acylation sites in human NOD2. Previous reports demonstrate that this mutant is predominantly cytosolic and that the Cys395 is minimally acylated in HEK293 cells [21]. However, it is unknown if this is because this mutant is a poor substrate or if it is more rapidly deacylated. Examining stable doxycycline-inducible GFP-NOD2^{L1007fs} in HCT116 cells reveals no plasma membrane localization and is unresponsive to ABHD17 inhibition (Figure 8*A*). Consistent with the microscopy data, using acyl-RAC, we detect no *S*-acylated protein in the presence or absence of ABD957 (Figure 8*B-C*); although this maneuver increased both wild-type and A755V S-acylation levels. These results suggest that GFP-NOD2^{L1007fs} is likely a poor substrate for ZDHHC5 and raises the possibility that Cys395 is acylated downstream of Cys1033 acylation.

Next, we examined three mutants residing within the central nucleotide-binding and oligomerization domain, also called the NACHT domain. Specifically, we examined the human variant A612V and two experimentally generated mutants, K305R and P486A. The K305R (Walker-A motif), P486A (GxP motif), and A612T (Walker-B motif)

mutations span the NACHT domain and are required for ATP binding and hydrolysis [42]. Using the Sleeping-Beauty doxycycline-inducible system, we examined the localization of GFP chimeras of these three mutants. Like the GFP-NOD2^{L1007fs}, these mutants display no plasma membrane localization in resting cells, which does not change after 4 hours of treatment with ABD957 (Figure 8*A*). Using acyl-RAC, these NACHT domain mutants show no basal *S*-acylation and no increase following incubation with ABD957, in contrast to wild-type or the A755V variant (Figure 8*B, C* and 6*E, H*). Consistent with previous reports [42], the K305R and P486A failed to activate the NF-κB pathway, and treatment with ABD957 could not increase signaling (Figure 8*D, E*). These results are consistent with the need for an initial ATP-binding and/or hydrolysis for NOD2 *S*-acylation.

DISCUSSION

The *S*-acylation of NOD2 attaches the protein to the plasma membrane, endosomes, and phagosomes critical for MDP-induced signaling [21]. Here, we demonstrate that ABHD17 enzymes remove the two acyl chains from NOD2, thus negatively regulating NOD2-mediated NF-κB signaling. The results further highlight how the S–acylation–deacylation cycle is a pivotal regulator of NOD2 function. Specific poorly *S*-acylated variants can be improved by targeting the ABHD17 family of thioesterases. This study further supports the previous findings that defective NOD2 *S*-acylation renders the protein non-functional in response to MDP and may contribute to CD's pathogenesis. Our findings also raise the possibility that approaches that attenuate the deacylation of NOD2 variants may be beneficial therapeutically depending on the

specific NOD2 mutation. It is worth noting that our work has been conducted in immortalized intestinal epithelial cells and HEK cells. This limitation could be mitigated by generating new mouse models or using CRISPR to generate iPSC cells with specific NOD2 variants for testing in organoid models.

This study investigated NOD2 loss-of-function variants associated with CD, including two more prevalent NOD2 mutations, L1007fs and R702W. The C-terminal truncation of 1007fs deletes one of the two *S*-acylation sites. Both these mutant proteins, in addition to L248R and A755V, are hypo-acylated and mislocalized in cells and have lost the ability to induce NF-κB signaling in response to MDP [21]. Although the previous study revealed some residual *S*-acylation of the FLAG-NOD2^{L1007fs} in Hela cells, we did not detect any in our system using the acyl-RAC assay. Furthermore, *S*-acylation was not increased in this mutant upon inhibition of ABHD17 isoforms. A few differences between the previous and current studies could result in differences. This includes different assays to assess *S*-acylation, different cell lines, and transient vs. stable inducible expression of the NOD2 proteins. However, the collective results demonstrate little to no *S*-acylation of the NOD2^{L1007fs} protein. Mechanistically, we can envisage a few possible explanations. First, the truncated protein is not recognized as a substrate by the ZDHHC5 enzyme. Second, there is a hierarchy in the order of *S*-acylation events, with Cys1033 being modified first and required for Cys395 to be acylated. Third, although our results suggest that ABHD17s are the primary thioesterases for NOD2, it is possible that a mono-*S*-acylated NOD2^{L1007fs} could be deacylated by another enzyme that usually doesn't recognize the dually *S*-acylated

NOD2 as a substrate. Regardless of the precise mechanism, it appears that the functionality of this mutant cannot be restored.

We observed improved *S*-acylation and plasmalemmal localization, and functionality in three hypo-acylated mutants, R702W, L248R and A755V. We also consistently found that the enhanced S-acylation also increase the phospho-IκB-α and a tendency to increase the secretion of cytokines in the HEK cells. In contrast, mutations within the NACHT domain display no *S*-acylation, which did not change with the inhibition of ABHD17 isoforms. It remains unknown which among the sixty CD-associated NOD2 variants are hypo-acylated and which could be improved through attenuation of ABHD17. Based on our findings, it is tempting to speculate that ZDHHC5 specifically recognizes and *S*-acylates the ATP-bound NOD2. Ultimately, we suspect that targeted inhibition of ABHD17 could benefit a subset of these human variants.

The connection between NOD2 loss-of-function mutants and CD may have significant implications for the disease. This is not only because dysfunction in the innate immune system is crucial in CD's development but also because it has been demonstrated that restoring normal innate signaling can alleviate colitis [43]. However, ongoing debates exist regarding how changes in NOD2 signaling can increase susceptibility to inflammation and the role post-transcriptional regulation plays in patients with or without NOD2 variants associated with the disease and their resulting pathogenic innate immune responses [44, 45]. *S*-acylation has been shown to impede autophagic degradation of NOD2 by attenuating binding to the cargo receptor p62/SQSTM1 [46]. The degradation rate is higher for *S*-acylation-deficient NOD2

variants than wild-type NOD2 [46, 47]. Thus, ABHD17 enzymes may also regulate NOD2 stability by coupling deacylation to its autophagic removal.

Additional roles for NOD2 have been described in response to viruses and ER stress. These roles for NOD2 do not require localization to the PM or endocytic organelles; instead, NOD2 redistributes to the mitochondria and ER. It is unclear whether these responses require *S*-acylated NOD2 or if ABHD17 isoforms will influence these pathways. Teleologically, both plasmalemmal (*S*-acylated) and cytosolic (non-acylated) pools of NOD2 may exist to allow NOD2 to function in many subcellular compartments under various stimuli and conditions. However, this requires further experimentation to assess this possibility.

ACKNOWLEDGEMENTS

The authors thank the Kennan Research Center for Biomedical Science Core Facilities at St. Michael's Hospital, especially Dr. Caterina di Ciano-Oliveira and Dr. Monika Lodyga, for their continued support, technical advice, expertise, and training.

AUTHOR CONTRIBUTIONS

Charneal Dixon investigation, formal analysis, manuscript first draft. **Noah Martin** investigation. **Micah Niphakis** resources. **Benjamin Cravatt** resources and funding acquisition. **Gregory Fairn** conceptualization, writing–review & editing, supervision, project administration, and funding acquisition.

RESOURCE AVAILABILITY

Lead contact

Further information and requests for resources and reagents should be directed to and will be fulfilled by the lead contact, Gregory Fairn (gfairn@dal.ca)

Materials availability

- Any plasmids or cell lines generated in this study are available upon request.

Data and code availability

- This paper does not report any original code.

- Any additional information required to reanalyze the data reported in this paper is available from the lead contact upon request.

METHODS

Reagents

L18-MDP (cat# tlrl-lmdp) was purchased from Invivogen (San Diego, USA). ML348 (cat# 899713-86-1), ML349 (cat# 890819-86-0), WWL70 (cat# 947669-91-2), orlistat (cat# 96829-58-2), *S*-Methyl thiomethanesulfonate (cat# 64306), sodium dodecyl sulfate (cat# 71736-500), hydroxylamine (cat# 159417), 4',6-diamidine-2'-phenylindole dihydrochloride (cat# 10236276001), NP-40 (cat# 492016-500L), Triton X-100 (cat# X-100) and puromycin (cat# P4512) were purchased from Sigma-Aldrich (Oakville, Canada). Palmostatin B (cat# 178501) and RIPA (cat# 20-188), products of EMD Millipore, were also purchased through Sigma-Aldrich (Oakville, Canada). Doxycycline hydrochloride (cat# DB0889) was obtained from BioBasic Inc. (Markham, Canada). High-capacity acyl-RAC S3 capture beads (cat# AR-S3-1) were purchased from NANOCS (Natick, USA).

Plasmids

ABHD17 (17A, 17B & 17C), ABHD6, ABHD12 and ABHD16A in pEF-BOS-HA were gifts of Dr. Jennifer Greaves (Research Centre for Health and Life Sciences, Coventry University, Coventry, U.K.). These plasmids encode full-length human ABHD17 (17A, 17B & 17C), ABHD6, ABHD12 and mouse ABHD16A. pSB-GFP-NOD2 was generated by cloning GFP-NOD2 into pSBTet-BP using two SfiI restriction sites on either side of the luciferase cassette. The NOD2 mutants were generated in this vector using the Q5 site-directed mutagenesis kit from New England Biolabs, resulting in single amino acid changes L248R, K305R, P486A, R702W, A612T, A755V and 3020insC in the expressed proteins.

Immortalized and engineered cell lines

Cells were purchased from the American Type Culture Collection (ATCC). Human colorectal carcinoma HCT116, HT29 and human embryonic kidney (HEK) 293T cell lines were maintained and propagated in high glucose Dulbecco's modification of Eagle's medium (DMEM) from Wisent (St. Bruno, Canada, cat# 319-020-CL) supplemented with 1.5 g/L sodium bicarbonate, L-glutamine and 10% fetal bovine serum (Wisent, cat# 080150) in a humidified incubator at 37 °C, 5% CO_2.

Stable cells were generated using the sleeping beauty transposon system [48]. To generate doxycycline-inducible stable integration of GFP-NOD2, cells were co-transfected with sleeping beauty vector (pSBTet-BP [48], Addgene # 60496) carrying the gene of interest and small amounts of the transposase encoding plasmid, pCMV(CAT)T7-SB100 [49] (Addgene # 34879). According to the manufacturer's instructions, cells were transfected using ViaFect transfection reagent (Promega,

Madison, WI). Forty-eight hours after transfection, cells were selected for puromycin resistance over 3-5 days and terminated when virtually all the cells displayed the expected doxycycline inducible GFP or constitutive BFP fluorescence. Expression of the GFP-NOD2 and the indicated mutants was induced using 1 µg/mL doxycycline unless otherwise indicated. Stable expression of GFP chimeric proteins was confirmed using microscopy and immunoblotting.

Transfections

cDNA transfections were performed using Promega ViaFect (cat# E4982), while siRNA transfections were performed using DharmaFECT2 (cat# T-2002-02) purchased from Horizon Discovery Biosciences. HCT116 cells were transfected with cDNAs as indicated in each experiment using ViaFect as per manufacturer's instructions. For immunofluorescence studies, HCT116 cells were grown on glass coverslips in 12-well plates and transfected at 60–80% confluence with 1 µg of cDNA per well for each of the indicated thioesterase encoding plasmids using Promega's Viafect according to product instructions.

Unless otherwise stated, for RNA interference experiments two rounds of transfection were used to introduce 100nM small interfering RNA in HCT116 and HEK293T on days 1 and 2 post-plating. For knockdown experiments, the ON-TARGETplus siRNA of targeted genes and the non-targeting siRNA were purchased from Horizon Discovery Biosciences. The silencer siRNA used are as follows: ON-TARGETplus Non-targeting siRNA, 5'-UGGUUUACAUGUCGACUAA- 3', ON-

TARGETplus Human ABHD17A siRNA, 5'-ACGUGAAAACGGAAAUUAA-3', ON-TARGETplus Human ABHD17C siRNA, 5'-CCACCAAUGUUCUCGGUAU-3', ON-TARGETplus SMARTpool Human ABHD17B siRNA (1# 5'-GGACUAGGAUCACGGAUUA-3', 2# 5'-GGAUCUUGCUGCUCGAUAU-3', 3# 5'-GUUCACCCAAUGCGAAAUA-3', 4# 5'-UCGCAUUGUUUGAACGUUG-3'). Since isoform-specific antibodies against ABHD17 isoforms are not available, RT-qPCR was used to quantify the degree of mRNA knockdown.

Experimentally, cells transfected with siRNA were induced with doxycycline on day 3, followed by confocal microscopy, cells were stimulated with L18-MDP on day 4, 18-20h following induction.

Inhibitor assays

Stable transfected HCT116 were cultured as monolayers on 18mm round glass coverslips in 12-well plates. Stable expression of GFP-tagged NOD2 or NOD2 variant was induced with doxycycline (1 µg/mL). Approximately 18-20h after induction, cells were treated with DMSO vehicle (control) or small molecule inhibitors Palmostatin B, Orlistat (tetrahydrolipstatin; THL), ABD957, WWL70, ML348, ML349 for 4 h at 37°C in 5% CO_2.

Preparation of cell extracts

Stable transfected HCT116 and HEK293T cells were induced with doxycycline (1 µg/mL) for 18-20 h, then treated with inhibitors or stimulated as indicated. Cells were harvested in phosphate-buffered saline (D-PBS; cat# 311-010-CL) from Wisent Inc., and lysed in RIPA buffer (CST; cat# 9806S) or NP-40 lysis buffer containing PhosSTOP phosphatase inhibitor (Roche; cat# 04906845001) and EDTA-free protease inhibitor

(BioShop; cat# PIC002-1) and incubated on ice for 1 hour, then centrifuged at 10,000 x*g* at 4°C for 10 minutes to obtain clear lysates. Protein concentration was determined with Pierce BCA protein assay (Thermo Scientific; cat# 23225).

Confocal microscopy

Cells were seeded on 18 mm-round glass coverslips in 12-well plates. Stable HCT116 cells expressing GFP-NOD2 wildtype and mutants were washed with PBS and fixed with a 4% paraformaldehyde solution for 20 min at room temperature. Glass coverslips were washed with PBS then incubated with 100 mM glycine, 0.1% v/v Triton X-100 for 20 min at room temperature. Cells were blocked with 5% BSA in PBS for 1h at room temperature and then probed with 1:100 anti-HA (CST) antibody overnight. The coverslips were washed three times with PBS, followed by a 1h incubation with species-matched 1:500 Cy5-conjugated goat anti-mouse IgG (Jackson ImmunoResearch) in PBS. Images were acquired in the St. Michael's Hospital Bioimaging Facility using a Zeiss Axiovert 200M microscope equipped with a Yokogawa CSU-X1 confocal spinning disc system and a 63X Apo PLAN VC, NA 1.40 oil objective and a Hamamatsu ImagEM X2 EM-CCD camera. Images were processed using ImageJ2 [50] version 2.14.0/1.54f.

Acyl resin-assisted-capture (Acyl-RAC) Stable HCT116 cells were harvested and lysed (1% Triton X-100, 50 mM Tris- HCl (pH 7.5), 150 mM NaCl, 1 mM EDTA, 1 % SDS, 0.5 % sodium deoxycholate, 1X protease inhibitor (BioShop; cat# PIC002-1), 0.2% v/v methyl methanethiosulfonate (MMTS). Lysates were sonicated and incubated at 42°C in a thermal shaker for 3h. Blocking was stopped, and MMTS was removed with 3-4 rounds of methanol/chloroform precipitation. The protein pellets were rinsed with methanol and air-dried. The pellets were redissolved in binding buffer (100 mM Tris- HCl

(pH 7.5), 1 mM EDTA, 1 % SDS) by incubating at 42°C in a thermal shaker, with intermittent mixing. The samples were sonicated in a water bath for 5-10 min to resuspend any undissolved pellet further. Each sample was divided in two, and 50 µL of hydroxylamine (NH2OH, 400 mM final concentration; or NaCl for control samples) was added before incubation with 25 µL of packed acyl-RAC beads (High-Capacity Acyl-RAC S3 beads; Nanocs # AR-S3-1,2) for 2 h at room temperature. The beads were washed 3 times with binding buffer before adding 4X SDS sample buffer with DTT and incubating the slurry at 80°C for 15 minutes.

RNA extraction and RT-qPCR

Total RNA was extracted from HCT116 cells RNeasy Mini Kit (cat# 74104; Qiagen, Germany) according to the manufacturer's protocols. cDNA was synthesized from 1 µg RNA using SensiFAST cDNA Synthesis (cat# BIO-65053; FroggaBio; Concord, Canada) and SensiFAST SYBR No-ROX kit (cat# BIO-98005). qPCR was performed using a BIO-RAD CFXOpus 96 Real-Time PCR System in conjunction with CFX Maestro software version 5.0.0.21.0616 (BIO-RAD; Ontario, Canada). All cycle threshold (CT) values were normalized to GAPDH. The relative expression level for each gene of interest was calculated using the $2^{-\Delta\Delta C_T}$ method [51]. The primer sequences were as follows: Human *ABHD17A* forward: 5'-ACCATCGAGGTCTTCCCCACCAGG-3', Human *ABHD17A* reverse: 5'-AGAAGAGGACCGTGTACCTGGCACC-3', Human *ABHD17B* forward: 5'-CCGCTCAGGTGCAGAGCATGAATAA-3', Human *ABHD17B* reverse: 5'-AAGCAATCTTCCCTGGACAAGGTGG-3', Human *ABHD17C* forward: 5'-TTGATGCTTTCCCCAGCATTGACA-3', Human *ABHD17C* reverse: 5'-TCGCTAGGCCATGGGAGAAATCG-3', Human *GAPDH* forward: 5'-CAATGACCCCTTCATTGACC-3', Human *GAPDH* reverse: 5'-

GACAAGCTTCCCGTTCTCAG-3', Human *NOD2* forward: 5'-GCACTGATGCTGGCAAAGAACG-3', Human *NOD2* reverse: 5'-CTTCAGTCCTTCTGCGAGAGAAC-3'.

Multiplex analysis of secreted cytokines

Using 12 well tissue culture plates, cells were cultured with DMEM containing 10% FBS. Cells were treated with siRNA complexes over 48 hours or ABD957 inhibitor for 4 hours, before brief stimulation with 100 ng/mL L18-MDP (1h for HEK293T cells and 6h for HCT116 cells). Plates were maintained at 37 °C in 5% CO_2 for 24 h. Next, supernatants were collected and analyzed using Luminex-100 MAP® technology for a panel of 14 human cytokines, chemokines, and growth factors. Specifically, plates were placed on ice, the contents of the wells for each condition (unstimulated, L18-MDP-stimulated) were transferred to 1.5mL microcentrifuge tubes, and samples were centrifuged at 4 °C for 10 min at 11,000 × *g* followed by distribution of the supernatant into 200 µl aliquots that were immediately frozen at −80 °C and maintained frozen until analysis. This was repeated 3 times to obtain 3 independent replicates. This multiplexing analysis was performed using a Luminex™ 200 system (Luminex, Austin, TX, USA) by Eve Technologies Corp. (Calgary, Alberta). Fourteen markers were simultaneously measured in the samples using Eve Technologies' Human High Sensitivity 14-Plex Discovery Assay® (MilliporeSigma, Burlington, Massachusetts, USA). The 14-plex consisted of GM-CSF, IFNγ, IL-1β, IL-2, IL-4, IL-5, IL-6, IL-8, IL-10, IL-12p70, IL-13, IL-17A, IL-23, TNF-α. Assay sensitivities of these markers range from 0.11 – 3.25 pg/mL for the 14-plex, and some samples required dilution for accurate determination. Individual analyte sensitivity values are available in the

MilliporeSigma MILLIPLEX® MAP protocol. Only molecules that reached the low end of the sensitivity are depicted in the results.

QUANTIFICATION AND STATISTICAL ANALYSIS

Statistical differences ($p<0.05$) were inferred using Student's two-tailed t-tests or one-way ANOVA with Dunnett's correction or two-way ANOVA with Fisher's least significant difference (LSD) method for multiple comparisons performed using Prism 10 (Graph-Pad Software, Inc., La Jolla, CA) with DMSO-treated, vector-co-transfected, or non-targeting siRNA-transfected samples as the control group. All significant differences are indicated in the text and figures. The statistical significance threshold was set to 0.05 throughout this study.

Cell membrane fluorescence intensity and immunoblot band intensities were quantified using ImageJ2 open-source image processing software.

REFERENCES

[1] Hampe J, Cuthbert A, Croucher PJ, Mirza MM, Mascheretti S, Fisher S, Frenzel H, King K, Hasselmeyer A, Macpherson AJ, Bridger S, Van Deventer S, Forbes A, Nikolaus S, Lennard-Jones JE, Foelsch UR, Krawczak M, Lewis C, Schreiber S, Mathew CG. Association between insertion mutation in NOD2 gene and Crohn's disease in German and British populations. The Lancet 2001;357(9272):1925-8.

[2] Hugot JP, Chamaillard M, Zouali H, Lesage S, Cézard JP, Belaiche J, Almer S, Tysk C, O'Morain CA, Gassull M, Binder V, Finkel Y, Cortot A, Modigliani R, Laurent-Puig P, Gower-Rousseau C, Macry J, Colombel JF, Sahbatou M, Thomas G. Association of NOD2 leucine-rich repeat variants with susceptibility to Crohn's disease. Nature 2001;411(6837):599-603.

[3] Ogura Y, Bonen DK, Inohara N, Nicolae DL, Chen FF, Ramos R, Britton H, Moran T, Karaliuskas R, Duerr RH, Achkar JP, Brant SR, Bayless TM, Kirschner BS, Hanauer SB, Nuñez G, Cho JH. A frameshift mutation in NOD2 associated with susceptibility to Crohn's disease. Nature 2001;411(6837):603-6.

[4] Caruso R, Warner N, Inohara N, Núñez G. NOD1 and NOD2: Signaling, Host Defense, and Inflammatory Disease. Immunity 2014;41(6):898-908.

[5] Franchi L, Warner N, Viani K, Nuñez G. Function of Nod-like receptors in microbial recognition and host defense. Immunological Reviews 2009;227(1):106-28.

[6] Ricardo, Milutinovic S, John. Roles of NOD1 (NLRC1) and NOD2 (NLRC2) in innate immunity and inflammatory diseases. Bioscience Reports 2012;32(6):597-608.

[7] Ogura Y, Inohara N, Benito A, Chen FF, Yamaoka S, Núñez G. Nod2, a Nod1/Apaf-1 Family Member That Is Restricted to Monocytes and Activates NF-κB. Journal of Biological Chemistry 2001;276(7):4812-8.

[8] Keestra AM, Bäumler AJ. Detection of enteric pathogens by the nodosome. Trends in Immunology 2014;35(3):123-30.

[9] Moreira LO, Zamboni DS. NOD1 and NOD2 Signaling in Infection and Inflammation. Frontiers in Immunology 2012;3.

[10] Grimm MC, Pavli P. NOD2 mutations and Crohn's disease: are Paneth cells and their antimicrobial peptides the link? Gut 2004;53(11):1558-60.

[11] Voss E, Wehkamp J, Wehkamp K, Stange EF, Schröder JM, Harder J. NOD2/CARD15 mediates induction of the antimicrobial peptide human beta-defensin-2. J Biol Chem 2006;281(4):2005-11.

[12] Hampe J, Franke A, Rosenstiel P, Till A, Teuber M, Huse K, Albrecht M, Mayr G, De La Vega FM, Briggs J, Günther S, Prescott NJ, Onnie CM, Häsler R, Sipos B, Fölsch UR, Lengauer T, Platzer M, Mathew CG, Krawczak M, Schreiber S. A genome-wide association scan of nonsynonymous SNPs identifies a susceptibility variant for Crohn disease in ATG16L1. Nat Genet 2007;39(2):207-11.

[13] Homer CR, Richmond AL, Rebert NA, Achkar JP, McDonald C. ATG16L1 and NOD2 interact in an autophagy-dependent antibacterial pathway implicated in Crohn's disease pathogenesis. Gastroenterology 2010;139(5):1630-41, 41.e1-2.

[14] Travassos LH, Carneiro LAM, Ramjeet M, Hussey S, Kim Y-G, Magalhães JG, Yuan L, Soares F, Chea E, Le Bourhis L, Boneca IG, Allaoui A, Jones NL, Nuñez G, Girardin SE, Philpott DJ. Nod1 and Nod2 direct autophagy by recruiting ATG16L1 to the plasma membrane at the site of bacterial entry. Nature Immunology 2010;11(1):55-62.

[15] Charrière GM, Ip WE, Dejardin S, Boyer L, Sokolovska A, Cappillino MP, Cherayil BJ, Podolsky DK, Kobayashi KS, Silverman N, Lacy-Hulbert A, Stuart LM. Identification of Drosophila Yin and PEPT2 as evolutionarily conserved phagosome-associated muramyl dipeptide transporters. J Biol Chem 2010;285(26):20147-54.

[16] Gutierrez O, Pipaon C, Inohara N, Fontalba A, Ogura Y, Prosper F, Nunez G, Fernandez-Luna JL. Induction of Nod2 in myelomonocytic and intestinal epithelial cells via nuclear factor-kappa B activation. J Biol Chem 2002;277(44):41701-5.

[17] Nakamura N, Lill JR, Phung Q, Jiang Z, Bakalarski C, De Mazière A, Klumperman J, Schlatter M, Delamarre L, Mellman I. Endosomes are specialized platforms for bacterial sensing and NOD2 signalling. Nature 2014;509(7499):240-4.

[18] Kim YG, Kamada N, Shaw MH, Warner N, Chen GY, Franchi L, Núñez G. The Nod2 sensor promotes intestinal pathogen eradication via the chemokine CCL2-dependent recruitment of inflammatory monocytes. Immunity 2011;34(5):769-80.
[19] Stafford CA, Gassauer A-M, De Oliveira Mann CC, Tanzer MC, Fessler E, Wefers B, Nagl D, Kuut G, Sulek K, Vasilopoulou C, Schwojer SJ, Wiest A, Pfautsch MK, Wurst W, Yabal M, Fröhlich T, Mann M, Gisch N, Jae LT, Hornung V. Phosphorylation of muramyl peptides by NAGK is required for NOD2 activation. Nature 2022;609(7927):590-6.
[20] Dixon CL, Fairn GD. S-palmitoylation of NOD2 controls its localization to the plasma membrane. Journal of Lipid Research 2021:100097.
[21] Lu Y, Zheng Y, Coyaud É, Zhang C, Selvabaskaran A, Yu Y, Xu Z, Weng X, Chen JS, Meng Y, Warner N, Cheng X, Liu Y, Yao B, Hu H, Xia Z, Muise AM, Klip A, Brumell JH, Girardin SE, Ying S, Fairn GD, Raught B, Sun Q, Neculai D. Palmitoylation of NOD1 and NOD2 is required for bacterial sensing. Science 2019;366(6464):7.
[22] Guan X, Fierke CA. Understanding Protein Palmitoylation: Biological Significance and Enzymology. Sci China Chem 2011;54(12):1888-97.
[23] He Y, Linder ME. Differential palmitoylation of the endosomal SNAREs syntaxin 7 and syntaxin 8. 2008;50(3):398-404.
[24] Lynch SJ, Snitkin H, Gumper I, Philips MR, Sabatini D, Pellicer A. The Differential Palmitoylation States of N-Ras and H-Ras Determine Their Distinct Golgi Subcompartment Localizations. 2015;230(3):610-9.
[25] Morrison E, Wegner T, Zucchetti AE, Álvaro-Benito M, Zheng A, Kliche S, Krause E, Brügger B, Hivroz C, Freund C. Dynamic palmitoylation events following T-cell receptor signaling. Communications Biology 2020;3(1).
[26] Barnich N, Aguirre JE, Reinecker H-C, Xavier R, Podolsky DK. Membrane recruitment of NOD2 in intestinal epithelial cells is essential for nuclear factor–κB activation in muramyl dipeptide recognition. Journal of Cell Biology 2005;170(1):21-6.
[27] Lé, Cine P, Esmiol S, Mé, Tais J-Y, Nicoletti C, Nourry C, McDonald C, Nunez G, Hugot J-P, Borg J-P, Ollendorff V. The NOD2-RICK Complex Signals from the Plasma Membrane. Journal of Biological Chemistry 2007;282(20):15197-207.
[28] Dekker FJ, Rocks O, Vartak N, Menninger S, Hedberg C, Balamurugan R, Wetzel S, Renner S, Gerauer M, Schölermann B, Rusch M, Kramer JW, Rauh D, Coates GW, Brunsveld L, Bastiaens PIH, Waldmann H. Small-molecule inhibition of APT1 affects Ras localization and signaling. Nature Chemical Biology 2010;6(6):449-56.
[29] Rusch M, Zimmermann TJ, Bürger M, Dekker FJ, Görmer K, Triola G, Brockmeyer A, Janning P, Böttcher T, Sieber SA, Vetter IR, Hedberg C, Waldmann H. Identification of acyl protein thioesterases 1 and 2 as the cellular targets of the Ras-signaling modulators palmostatin B and M. Angew Chem Int Ed Engl 2011;50(42):9838-42.
[30] Lin DTS, Conibear E. ABHD17 proteins are novel protein depalmitoylases that regulate N-Ras palmitate turnover and subcellular localization. eLife 2015;4.
[31] Cao Y, Qiu T, Kathayat RS, Azizi SA, Thorne AK, Ahn D, Fukata Y, Fukata M, Rice PA, Dickinson BC. ABHD10 is an S-depalmitoylase affecting redox homeostasis through peroxiredoxin-5. Nat Chem Biol 2019;15(12):1232-40.

[32] Bononi G, Tuccinardi T, Rizzolio F, Granchi C. α/β-Hydrolase Domain (ABHD) Inhibitors as New Potential Therapeutic Options against Lipid-Related Diseases. Journal of Medicinal Chemistry 2021;64(14):9759-85.
[33] Savinainen JR, Patel JZ, Parkkari T, Navia-Paldanius D, Marjamaa JJ, Laitinen T, Nevalainen T, Laitinen JT. Biochemical and pharmacological characterization of the human lymphocyte antigen B-associated transcript 5 (BAT5/ABHD16A). PLoS One 2014;9(10):e109869.
[34] Won SJ, Davda D, Labby KJ, Hwang SY, Pricer R, Majmudar JD, Armacost KA, Rodriguez LA, Rodriguez CL, Chong FS, Torossian KA, Palakurthi J, Hur ES, Meagher JL, Brooks CL, Stuckey JA, Martin BR. Molecular Mechanism for Isoform-Selective Inhibition of Acyl Protein Thioesterases 1 and 2 (APT1 and APT2). ACS Chemical Biology 2016;11(12):3374-82.
[35] Li W, Blankman JL, Cravatt BF. A functional proteomic strategy to discover inhibitors for uncharacterized hydrolases. J Am Chem Soc 2007;129(31):9594-5.
[36] Navia-Paldanius D, Savinainen JR, Laitinen JT. Biochemical and pharmacological characterization of human α/β-hydrolase domain containing 6 (ABHD6) and 12 (ABHD12). J Lipid Res 2012;53(11):2413-24.
[37] Kamat SS, Camara K, Parsons WH, Chen DH, Dix MM, Bird TD, Howell AR, Cravatt BF. Immunomodulatory lysophosphatidylserines are regulated by ABHD16A and ABHD12 interplay. Nat Chem Biol 2015;11(2):164-71.
[38] Remsberg JR, Suciu RM, Zambetti NA, Hanigan TW, Firestone AJ, Inguva A, Long A, Ngo N, Lum KM, Henry CL, Richardson SK, Predovic M, Huang B, Dix MM, Howell AR, Niphakis MJ, Shannon K, Cravatt BF. ABHD17 regulation of plasma membrane palmitoylation and N-Ras-dependent cancer growth. Nature Chemical Biology 2021;17(8):856-64.
[39] Al Nabhani Z, Dietrich G, Hugot J-P, Barreau F. Nod2: The intestinal gate keeper. PLOS Pathogens 2017;13(3):e1006177.
[40] Strober W, Watanabe T. NOD2, an intracellular innate immune sensor involved in host defense and Crohn's disease. Mucosal Immunology 2011;4(5):484-95.
[41] Weichart D, Gobom J, Klopfleisch S, Häsler R, Gustavsson N, Billmann S, Lehrach H, Seegert D, Schreiber S, Rosenstiel P. Analysis of NOD2-mediated Proteome Response to Muramyl Dipeptide in HEK293 Cells. Journal of Biological Chemistry 2006;281(4):2380-9.
[42] Zurek B, Proell M, Wagner RN, Schwarzenbacher R, Kufer TA. Mutational analysis of human NOD1 and NOD2 NACHT domains reveals different modes of activation. Innate Immunity 2012;18(1):100-11.
[43] Watanabe T, Asano N, Murray PJ, Ozato K, Tailor P, Fuss IJ, Kitani A, Strober W. Muramyl dipeptide activation of nucleotide-binding oligomerization domain 2 protects mice from experimental colitis. J Clin Invest 2008;118(2):545-59.
[44] Salem M, Seidelin JB, Rogler G, Nielsen OH. Muramyl dipeptide responsive pathways in Crohn's disease: from NOD2 and beyond. Cell Mol Life Sci 2013;70(18):3391-404.
[45] Strober W, Asano N, Fuss I, Kitani A, Watanabe T. Cellular and molecular mechanisms underlying NOD2 risk-associated polymorphisms in Crohn's disease. Immunol Rev 2014;260(1):249-60.

[46] Zhou L, Zeng H, Cui J, Jin S. Palmitoylation facilitates inflammation through suppressing NOD2 degradation mediated by the selective autophagy receptor SQSTM1. Autophagy 2022;18(9):2254-5.
[47] Zhou L, He X, Wang L, Wei P, Cai Z, Zhang S, Jin S, Zeng H, Cui J. Palmitoylation restricts SQSTM1/p62-mediated autophagic degradation of NOD2 to modulate inflammation. Cell Death & Differentiation 2022.
[48] Kowarz E, Löscher D, Marschalek R. Optimized Sleeping Beauty transposons rapidly generate stable transgenic cell lines. Biotechnology Journal 2015;10(4):647-53.
[49] Mátés L, Chuah MK, Belay E, Jerchow B, Manoj N, Acosta-Sanchez A, Grzela DP, Schmitt A, Becker K, Matrai J, Ma L, Samara-Kuko E, Gysemans C, Pryputniewicz D, Miskey C, Fletcher B, VandenDriessche T, Ivics Z, Izsvák Z. Molecular evolution of a novel hyperactive Sleeping Beauty transposase enables robust stable gene transfer in vertebrates. Nat Genet 2009;41(6):753-61.
[50] Rueden CT, Schindelin J, Hiner MC, DeZonia BE, Walter AE, Arena ET, Eliceiri KW. ImageJ2: ImageJ for the next generation of scientific image data. BMC Bioinformatics 2017;18(1):529.
[51] Livak KJ, Schmittgen TD. Analysis of relative gene expression data using real-time quantitative PCR and the 2(-Delta Delta C(T)) Method. Methods 2001;25(4):402-8.

FIGURE LEGENDS

Figure 1. Inhibiting acyl protein thioesterases increases plasmalemmal NOD2 and *S*-acylation (*A*) Immunoblot showing doxycycline-inducible expression of GFP-NOD2 and GAPDH in HCT116 cells. (*B*) Low magnification epifluorescence micrographs of GFP-NOD2 in HCT116 cells following induction with 1 µg/mL doxycycline for 18 h. Scale bar, 100 µm. (*C*) Confocal microscopy of human colorectal carcinoma cells HCT116 and HT29 expressing stably transfected GFP-NOD2 (pseudo-colored cyan). Cells were treated with 100 µM palmostatin B (PalmB) or dimethyl sulfoxide (DMSO, vehicle) for 4 h. Scale bars, 10µm. (*D*) Quantification of plasma membrane localization and the effect of PalmB on GFP-NOD2 in HCT116 (*D*) and HT29 (*E*) cells from images as in (*C*). (*F*) *S*-acylation levels of GFP-NOD2 expressed in HCT116 cells treated with DMSO or PalmB. *S*-acylated GFP-NOD2 was detected in total cell lysates using acyl resin-

assisted-capture (acyl-RAC) assay and immunoblot analysis; samples omitting hydroxylamine (HA) are used as a control to demonstrate the fidelity of the assay specificity. (*G*) Quantification of *S*-acylation assay depicted in (*F*). (*H*) Average fold change quantification for quantification shown in (G). All data are representative of at least three independent experiments, with means indicated by a horizontal black line and samples from individual replicates color-matched. Unpaired two-tailed Student's t-test determined P-values for data in D, E, and G; p≤0.05 (*) and p≤0.0001 (****).

Figure 2. ABHD17 isoforms mediate enzymatic deacylation of NOD2. (*A, G*) Confocal images showing localization of GFP-NOD2 (A) and GFP-NOD1 (G) in HCT116 cells treated with selective small molecule acyl thioesterase inhibitors: 2.5 μM ABD957, 50 μM ML348 or 40 μM ML349 for 4 h. GFP-NOD2 expressing cells were also treated with 40 μM orlistatin (THL) and 25 μM WWL70. Scale bars, 10μm. (*B, H*) Quantification of GFP-NOD2 and GFP-NOD1 plasma membrane localization from images as in (*A, G*). (*C*) Confocal images showing localization of GFP-NOD2 in HT29 cells treated with 2.5 μM ABD957. (*D*) Quantification of GFP-NOD2 plasma membrane localization from representative images as in (C) in HT29 cells treated with ABD957 or DMSO. (*E, F*) Acyl-RAC analysis of GFP-NOD2 in HCT116 cells treated with THL, ABD957 or PalmB. All data are representative of at least three independent experiments, with means indicated by a horizontal black line and samples from individual replicates color-matched. Statistical significance was determined by two-tailed Student's unpaired *t*-test or one-way ANOVA followed by Dunnett's *post hoc* test. Group differences were considered significant for p≤0.05 (*), p≤0.01 (**) and p≤0.0001 (****). Not significant; *ns*.

Figure 3. Enforced expression of ABHD17 decreases NOD1 and NOD2 plasma membrane localization. (*A*) Confocal images of stable HCT116/GFP-NOD2 (cyan) cells transiently transfected with 3HA-tagged α/β-hydrolase domain (ABHD) 6, 12, 16A, 17A, 17B and 17C enzymes (greyscale). (*B*) Quantification of GFP-NOD2 plasma membrane localization from images as in *A*. (*C*) Confocal images of stable HCT116/NOD1 (cyan) transiently transfected with 3HA-tagged ABHD17 isoforms (greyscale). Asterisks (*) indicate GFP-NOD1 and ABHD17 co-transfected cells. All data are representative of at least three independent experiments, with means indicated by a horizontal black line and samples from individual replicates color-matched. P-values for B-D and F-H were determined by ordinary one-way ANOVA followed by Dunnett's multiple comparison test.; p≤0.01 (**), p≤0.0001 (****). Not significant; *ns*. Scale bars, 10 µm.

Figure 4. SiRNA-mediated ABHD17 knockdown enhances the plasmalemmal localization of GFP-NOD2 in HCT116 cells. (*A*) Quantitation of mRNA abundance for *NOD2, ABHD17A*, *ABHD17B* and *ABHD17C* gene expression relative to *GAPDH* ($2^{-\Delta CT}$) in HCT116 cells. (*B*) RT-qPCR of *ABHD17A*, *ABHD17B,* and *ABHD17C* transcript levels in HCT116 cells treated with small interfering RNA (siRNA): non-targeting (grey), ABHD17A (cyan), ABHD17B (orange), ABHD17 C(yellow) or a mixture of all three siRNAs targeting ABHD17A-C (magenta) for 48h. (*C***)** Confocal images of GFP-NOD2 in HCT116 treated with the indicated siRNAs. Scale bars, 10µm. (*D*) Quantification of GFP-NOD2 plasma membrane localization from images as in *C*. All data are representative of at least three independent experiments. Mean values ± SD in *A*. p-values for data in *D*

were determined by one-way ANOVA followed by Dunnett's multiple comparisons tests. Group differences were considered significant for p≤0.05 (*), p≤0.001 (***) and p≤0.0001 (****). Not significant; *ns*.

Figure 5. SiRNA-mediated ABHD17 knockdown enhances NOD2 signaling in HCT116 cells. (*A*) Immunoblots of phosphorylated- IkBα, NF-κB p65, and MAPK p38 in HCT116 cells. (B-D) Quantification of immunoblots as in A. (*E-H*) Cytokine (GM-CSF and IL-8) levels in cell culture supernatants. All data are representative of at least three independent experiments. All error bars, mean values ± SD. P-values for data in *B, C* & *D* were determined by one-way ANOVA followed by Tukey's multiple comparisons test. Statistical significance of data in E, F, G & H was determined by two-way ANOVA then Šídák's multiple comparisons test. Group differences were considered significant for p≤0.05 (*), p≤0.01 (**), p≤0.001 (***) and p≤0.0001 (****). Not significant; *ns*.

Figure 6. Inhibition of ABHD17 enzymes partly restores *S*-acylation of defective NOD2 variants. (*A*) Confocal images of doxycycline-inducible GFP-tagged human NOD2 variants L248R, R702W, and A755V in HCT116 cells. Cells were treated with solvent control, 40 μM THL, 100 μM PalmB, 2.5 μM ABD957, or a combination of siRNAs targeting ABHD17A, B, C (triple KD). Scale bars, 10 μm. (*B-D*) Quantification of plasma membrane localization of the GFP-NOD2 variants from images as in *A*. (*E-H*) *S*-acylation levels of NOD2 variants L248R, R702W and A755V in HCT116 cells treated with THL, ABD957 or PalmB. All data are representative of at least three independent experiments. Data are mean values ± SD. P-values for data in *B, C, D,* F, G & H were

determined by one-way ANOVA followed by Dunnett's multiple comparisons test. Group differences were considered significant for p≤0.05 (*), p≤0.01 (**), p≤0.001 (***) and p≤0.0001 (****). Not significant; *ns*.

Figure 7. Targeting ABHD17 isoforms improves the functionality of select Crohn's disease-associated NOD2 variants. (*A*) Detection of phosphorylated-IKB and phosphorylated-p38 MAPK using immunoblotting with the No Stain total protein stain. Whole-cell lysates of HEK293T cells stably expressing (*A*) L248R (*B*) R702W (*C*) A755V were simulated with L18-MDP for 1h after being treated with either DMSO, ABD957, or siRNAs. Cytokine levels (*D*) IL-8 and (*E*) TNFα in cell culture supernatants. All data and immunoblots are representative of at least three independent experiments. Data represents the mean ± SD. Significance of *D* & *E* was assessed by calculating P-values of the using two-way ANOVA then Šídák's multiple comparisons test. Group differences were considered significant for p≤0.0001 (****). Not significant; *ns*.

Figure 8. NOD2^{L1007fs} and NACHT mutants are not *S*-acylated or improved by targeting ABHD17 enzymes in HCT116 cells. (*A*) Confocal images of HCT116 cells stably transfected with doxycycline-inducible NOD2 variants: L1007fs and three NACHT/nucleoside-triphosphatase domain mutants, the human variant A612T, and two experimentally generated mutants K305R and P486A treated with DMSO or ABD957 for 4 hours. (*B*) S-acylation of wild-type NOD2 and the indicated mutants treated with ABD957 inhibitor using acyl-RAC and immunoblotting. Note: wild-type and A755V are used as positive controls in this experiment. (*C*) Quantification of panel *B* from three

independent experiments. (*D*) HEK293T cells transiently expressing wt-NOD2 and the indicated variants were incubated with ABD957 +/- MDP for 1 h. Whole cell lysates were resolved and phosphorylated-IKB was detected by immunoblotting. All data are representative of at least three independent experiments and samples from individual replicates color-matched. An unpaired two-tailed Student's t-test was used to compare the solvent control and ABD957 conditions for wt-NOD2 and each variant in *C* & *E*; Group differences were considered significant for $p \leq 0.05$ (*), $p \leq 0.01$ (**) and $p \leq 0.0001$. Not significant; *ns*.

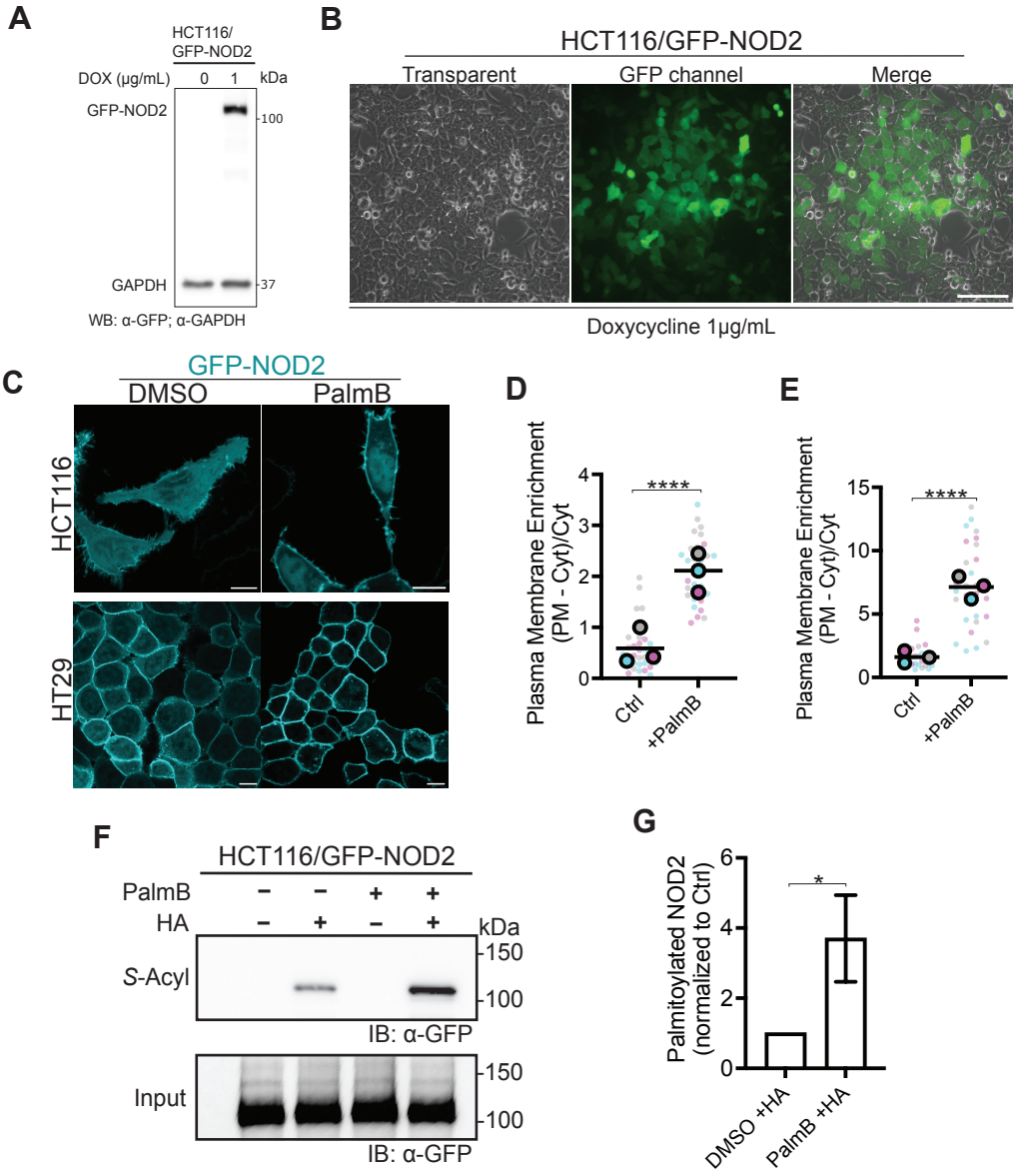
A
HCT116/
GFP-NOD2
DOX (μg/mL)
0
1
kDa
GFP-NOD2
100
GAPDH
37
WB: α-GFP; α-GAPDH
B
HCT116/GFP-NOD2
Transparent
GFP channel
Merge
Doxycycline 1μg/mL
C
GFP-NOD2
DMSO
PalmB
HCT116
HT29
D
Plasma Membrane Enrichment
(PM - Cyt)/Cyt
****
Ctrl
+PalmB
E
Plasma Membrane Enrichment
(PM - Cyt)/Cyt
****
Ctrl
+PalmB
F
HCT116/GFP-NOD2
PalmB
HA
kDa
S-Acyl
150
100
IB: α-GFP
Input
150
100
IB: α-GFP
G
Palmitoylated NOD2
(normalized to Ctrl)
*
DMSO +HA
PalmB +HA

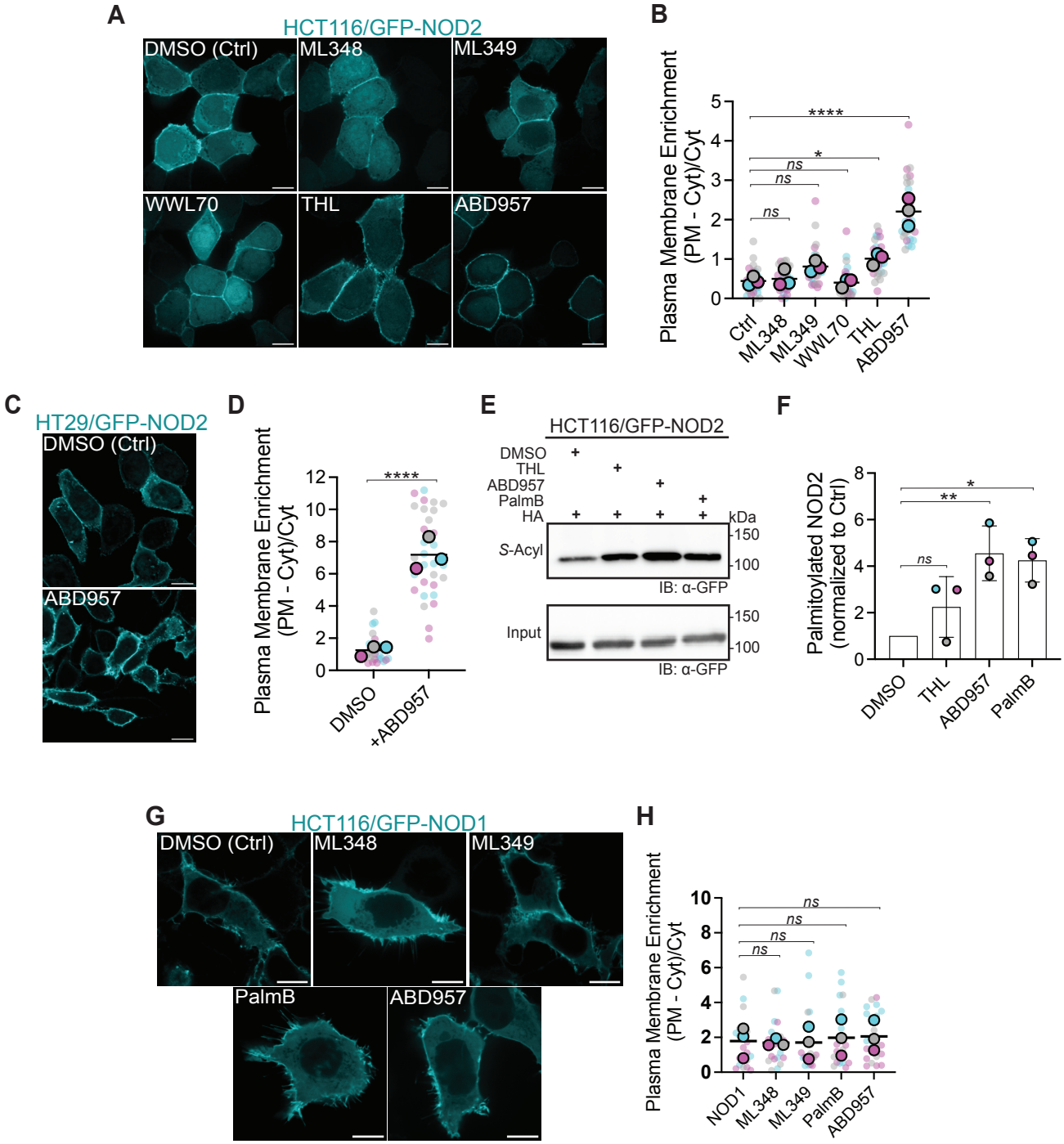
A
HCT116/GFP-NOD2
DMSO (Ctrl)
ML348
ML349
WWL70
THL
ABD957
B
Plasma Membrane Enrichment (PM - Cyt)/Cyt
****
*
ns
ns
ns
Ctrl
ML348
ML349
WWL70
THL
ABD957
C
HT29/GFP-NOD2
DMSO (Ctrl)
ABD957
D
Plasma Membrane Enrichment (PM - Cyt)/Cyt
****
DMSO
+ABD957
E
HCT116/GFP-NOD2
DMSO
THL
ABD957
PalmB
HA
kDa
S-Acyl
150
100
IB: α-GFP
Input
150
100
IB: α-GFP
F
Palmitoylated NOD2 (normalized to Ctrl)
*
**
ns
DMSO
THL
ABD957
PalmB
G
HCT116/GFP-NOD1
DMSO (Ctrl)
ML348
ML349
PalmB
ABD957
H
Plasma Membrane Enrichment (PM - Cyt)/Cyt
ns
ns
ns
ns
NOD1
ML348
ML349
PalmB
ABD957

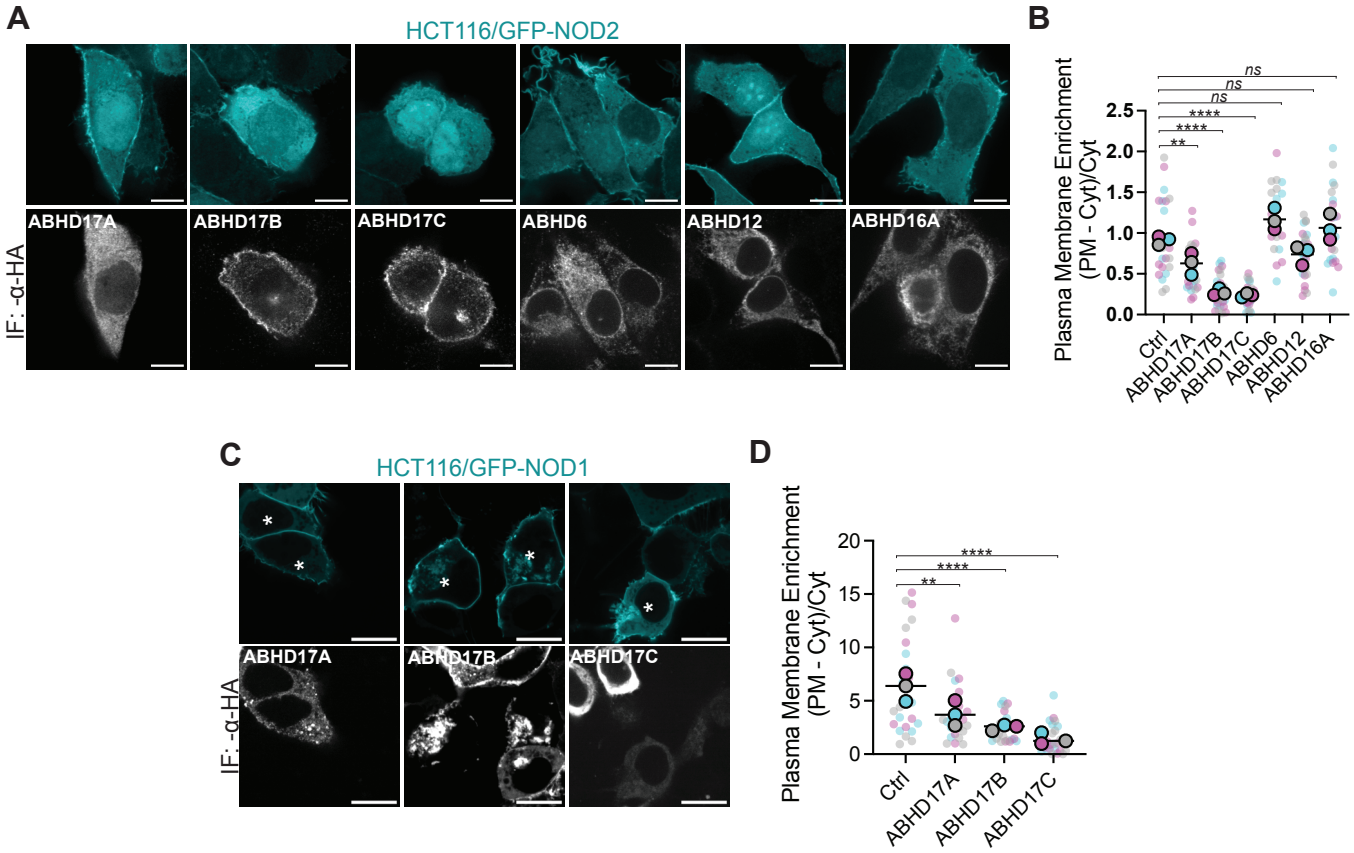
A
HCT116/GFP-NOD2
IF: -α-HA
ABHD17A
ABHD17B
ABHD17C
ABHD6
ABHD12
ABHD16A
B
Plasma Membrane Enrichment (PM - Cyt)/Cyt
ns
ns
ns
****
****
**
Ctrl
ABHD17A
ABHD17B
ABHD17C
ABHD6
ABHD12
ABHD16A
C
HCT116/GFP-NOD1
IF: -α-HA
ABHD17A
ABHD17B
ABHD17C
D
Plasma Membrane Enrichment (PM - Cyt)/Cyt
****
****
**
Ctrl
ABHD17A
ABHD17B
ABHD17C

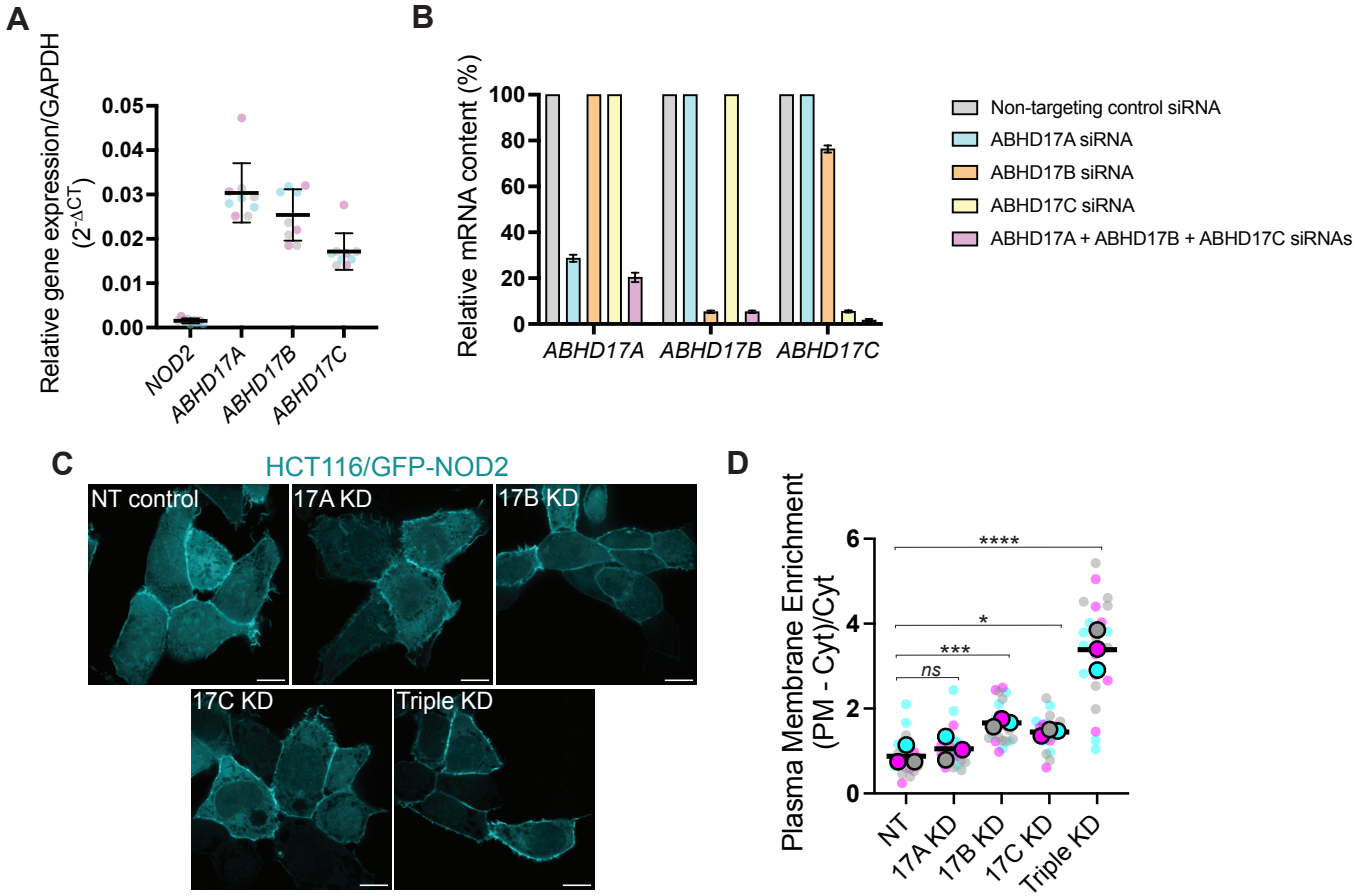
A
Relative gene expression/GAPDH
(2^-ΔCT)
0.05
0.04
0.03
0.02
0.01
0.00
NOD2
ABHD17A
ABHD17B
ABHD17C
B
Relative mRNA content (%)
100
80
60
40
20
0
ABHD17A
ABHD17B
ABHD17C
Non-targeting control siRNA
ABHD17A siRNA
ABHD17B siRNA
ABHD17C siRNA
ABHD17A + ABHD17B + ABHD17C siRNAs
C
HCT116/GFP-NOD2
NT control
17A KD
17B KD
17C KD
Triple KD
D
Plasma Membrane Enrichment
(PM - Cyt)/Cyt
6
4
2
0
****
*
***
ns
NT
17A KD
17B KD
17C KD
Triple KD

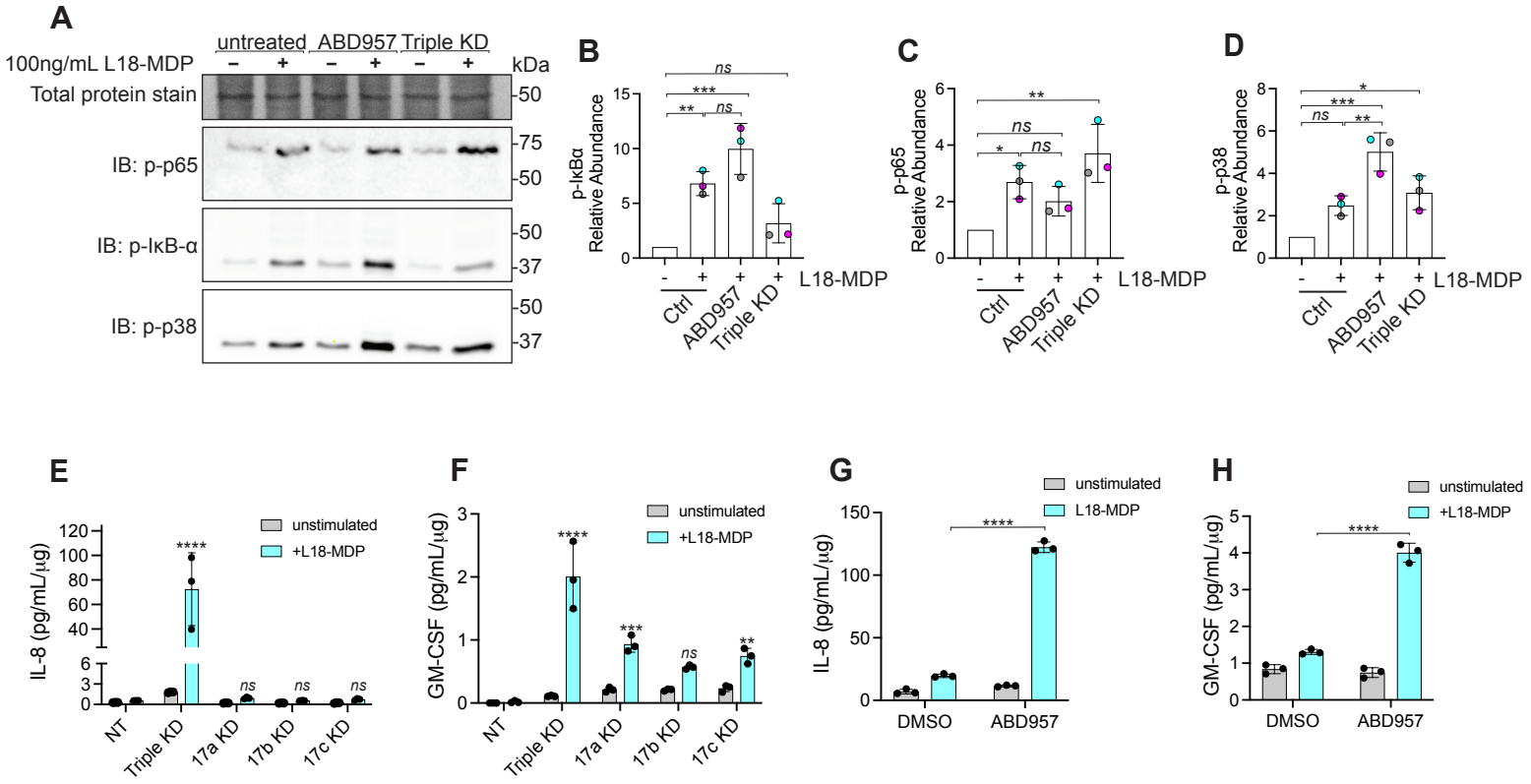
A
untreated
ABD957
Triple KD
100ng/mL L18-MDP
kDa
Total protein stain
IB: p-p65
IB: p-IκB-α
IB: p-p38
B
p-IκBα Relative Abundance
L18-MDP
Ctrl
ABD957
Triple KD
C
p-p65 Relative Abundance
D
p-p38 Relative Abundance
E
IL-8 (pg/mL/μg)
unstimulated
+L18-MDP
NT
Triple KD
17a KD
17b KD
17c KD
F
GM-CSF (pg/mL/μg)
G
L18-MDP
DMSO
ABD957
H

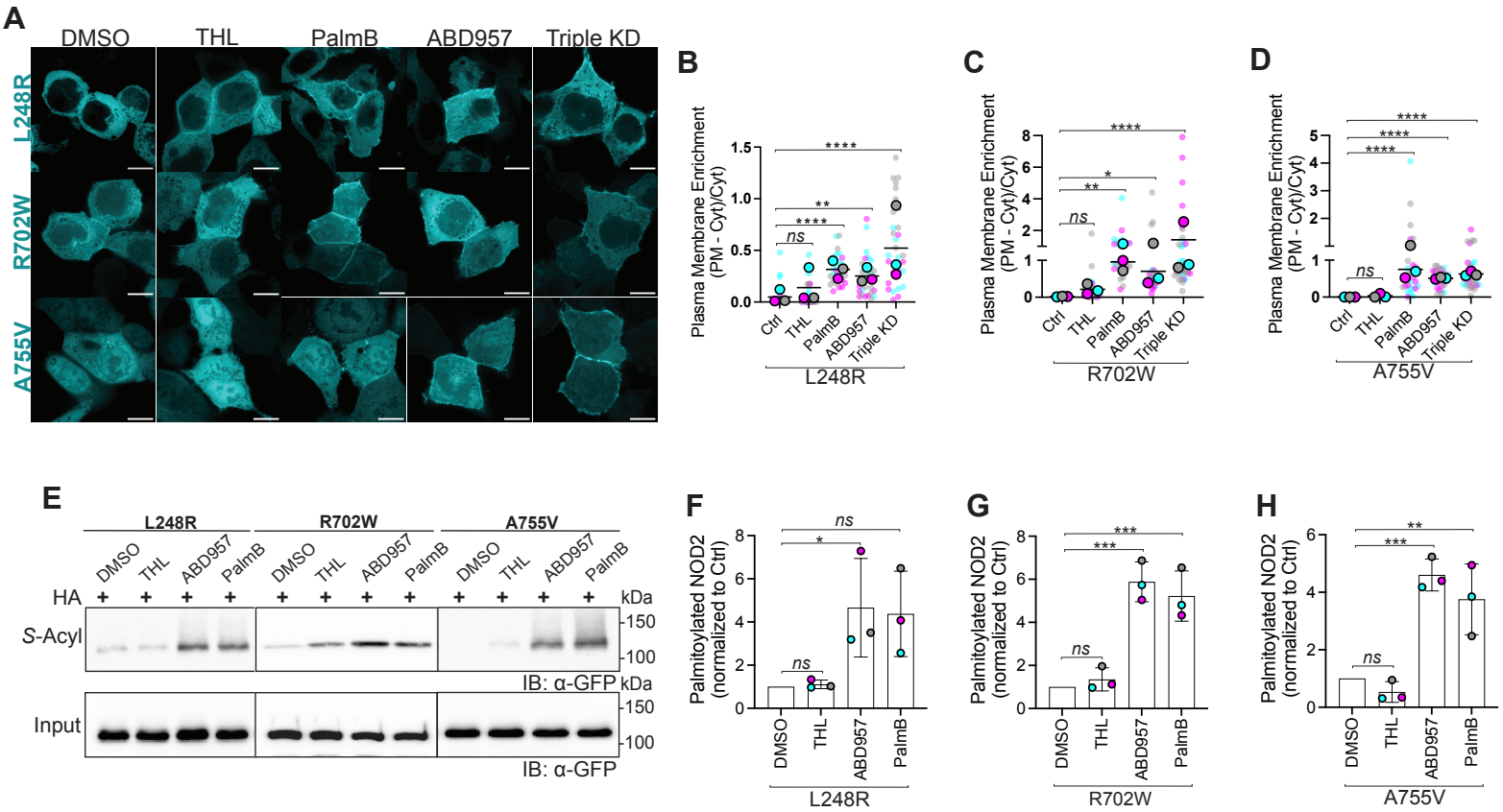
A
DMSO
THL
PalmB
ABD957
Triple KD
L248R
R702W
A755V
B
Plasma Membrane Enrichment (PM - Cyt)/Cyt)
ns
**
****
Ctrl
THL
PalmB
ABD957
Triple KD
L248R
C
Plasma Membrane Enrichment (PM - Cyt)/Cyt)
ns
**
*
****
R702W
D
Plasma Membrane Enrichment (PM - Cyt)/Cyt)
ns
****
A755V
E
L248R
R702W
A755V
DMSO
THL
ABD957
PalmB
HA
S-Acyl
Input
kDa
150
100
IB: α-GFP
F
Palmitoylated NOD2 (normalized to Ctrl)
ns
*
L248R
G
Palmitoylated NOD2 (normalized to Ctrl)
ns
***
R702W
H
Palmitoylated NOD2 (normalized to Ctrl)
ns
**
***
A755V

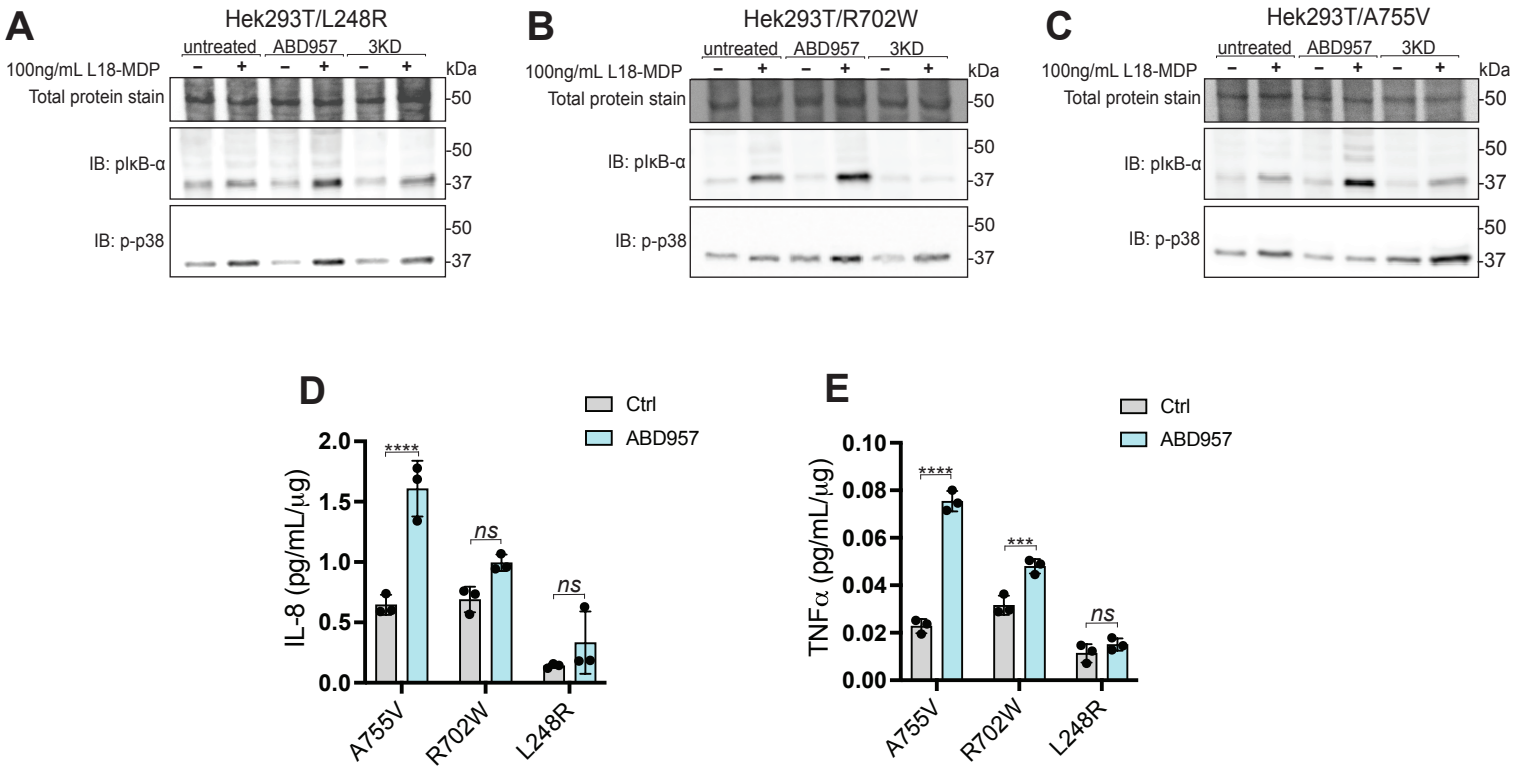
A
Hek293T/L248R
untreated
ABD957
3KD
100ng/mL L18-MDP
kDa
Total protein stain
IB: pIκB-α
IB: p-p38
B
Hek293T/R702W
C
Hek293T/A755V
D
Ctrl
ABD957
IL-8 (pg/mL/μg)
****
ns
A755V
R702W
L248R
E
TNFα (pg/mL/μg)
***

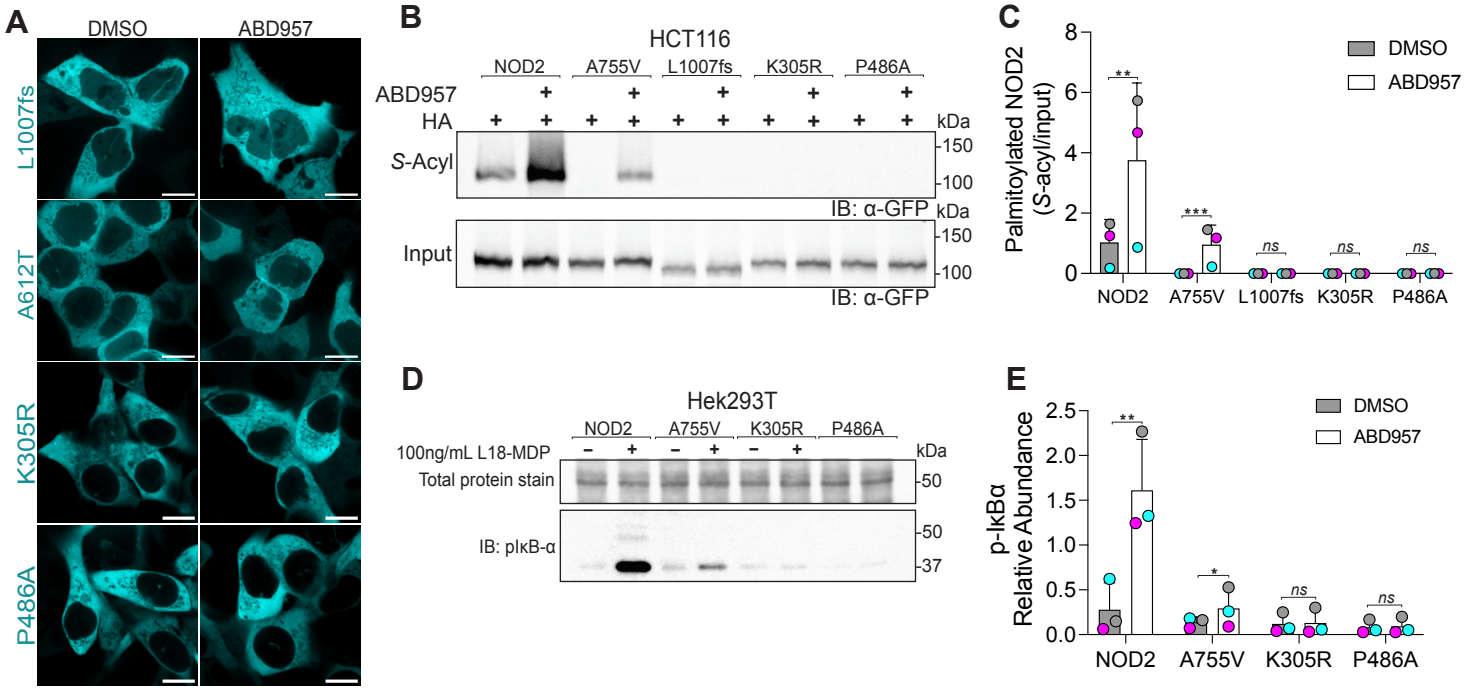
A
DMSO
ABD957
L1007fs
A612T
K305R
P486A
B
HCT116
NOD2
A755V
L1007fs
K305R
P486A
ABD957
HA
kDa
S-Acyl
150
100
IB: α-GFP
Input
C
Palmitoylated NOD2 (S-acyl/input)
DMSO
ABD957
**
***
ns
D
Hek293T
100ng/mL L18-MDP
Total protein stain
IB: pIκB-α
50
37
E
p-IκBα Relative Abundance
*